The Pennsylvania State University

The Graduate School

College of Engineering

# CFD ANALYSIS OF OZONE REACTION WITH HUMAN SURFACE: INFLUENCE OF INDOOR AIR FLOW CONDITIONS AND SURFACE REACTIVITY

A Thesis in

Aerospace Engineering

by

Sagar Sangameswaran Ananthanarayanan



Submitted in Partial Fulfillment
of the Requirements
for the Degree of

Master of Science

August 2016

The thesis of Sagar Sangameswaran Ananthanarayanan was reviewed and approved* by the following:

Donghyun Rim
Assistant Professor of Architectural Engineering
Thesis Co-Advisor

Susan Stewart
Senior Research Associate and Associate Professor of Aerospace Engineering & Architectural Engineering
Thesis Co-Advisor

George A. Lesieutre
Professor of Aerospace Engineering
Head of the Department of Aerospace Engineering

*Signatures are on file in the Graduate School

# ABSTRACT

Ozone reaction with the human body surface can significantly influence breathing zone ozone concentrations. Human exposure to ozone and its reaction products may also adversely affect health and comfort. Ozone uptake to indoor surfaces has been characterized for many building materials; however, limited information is available on how ozone reaction with human surface is influenced by human surface reactivity and airflow around human body. The objectives of this study are 1) to investigate ozone reaction with human surfaces depending on indoor ventilation conditions; 2) to examine the breathing zone concentration of ozone considering reactivity of human skin oil and clothing; and 3) to explore the effect of reaction probability on ozone mass transfer rate.

A computational fluid dynamics (CFD) simulation was verified and validated with previously published chamber experiments. The validated CFD models were applied further to examine the ozone reaction with the human surface in varying airflow conditions. Effects of varying degrees of human surface reactivity on the breathing zone concentration were examined.

For typical indoor environments with air change rate < 5 $h^{-1}$, the ozone mass transfer rate (deposition velocity) was in the range of 8-10 m/h with perfect sink condition. Parametric analysis results reveal that surface reactivity of the human body has a larger influence than air change rate and ventilation pattern. The breathing zone ozone concentration is also strongly influenced by surface reactivity. With a supply ozone concentration of 100 ppb and a transport-limited rate at the human surface (such as human skin oil), the breathing zone concentrations are in the range of 81-97 ppb, while the range is 96-99 ppb with lower surface reaction rate.

These results imply that the reaction probability of the human surface has a significant impact on human exposure to ozone and reaction byproducts.

# TABLE OF CONTENTS

# LIST OF FIGURES

# LIST OF TABLES

# LIST OF APPENDIX FIGURES

# ACKNOWLEDGEMENTS

I express my heartfelt gratitude to my co-advisor, Dr. Donghyun Rim, for his prized guidance, expertise and support through every phase of my research.

I wish to record my gratefulness to my co-advisor, Dr. Susan Stewart, for her kindness and valuable assistance during times of need.

I would also like to thank Dr. George A. Lesieutre, for providing the opportunity to earn Master of Science degree in Aerospace Engineering at the Pennsylvania State University.

# NOMENCLATURE

## Abbreviations

| | |
|---|---|
| CFD | Computational fluid dynamics |
| UV | Ultraviolet |
| VOCs | Volatile organic compounds |
| U.S. EPA | United States Environmental Protection Agency |
| ORPHS | Ozone reaction products associated with human surfaces |
| SST | Shear stress transport |
| ppb | Parts per billion |
| ppm | Parts per million |
| ACH | Air changes per hour |

## Symbols

| | | |
|---|---|---|
| $v_d$ | Deposition velocity | m/h |
| $C_s$ | Supply concentration | ppb |
| $C_{ex}$ | Exhaust concentration | ppb |
| $C_b$ | Bulk/ambient concentration | ppb |
| $Q$ | Volumetric flow rate | $m^3/h$ |
| $A_h$ | Area of human surface | $m^2$ |
| $A_i$ | Age of air at location $i$ | min |
| $C_i$ | Concentration at location $i$ | ppb |

| | | |
|---|---|---|
| $v_t$ | Transport-limited deposition velocity | cm/s |
| $\gamma$ | Reaction probability | |
| $\langle v \rangle$ | Boltzmann velocity | cm/s |

# Chapter 1

# Introduction

## Ozone and health effects

Ozone is a colorless and odorless gas, which serves as a protective shield against the sun's harmful ultraviolet (UV) radiation in the stratosphere (Devlin et al., 1997). However, in the troposphere, the very same compound can act as a pollutant with a multitude of potential associated adverse health effects. The majority of ground-level ozone is formed when nitrogen oxides (NOx), carbon monoxide (CO), and volatile organic compounds (VOCs) comprised mainly of hydrocarbons react in the presence of UV radiation from the sun (Comrie, 1990; Devlin et al., 1997). Even low levels (20 ppb) of ozone exposure can cause adverse health symptoms such as coughing, chest pain, shortness of breath, wheezing, throat irritation, airway inflammation and asthma (Lippmann, 1989; U.S. EPA, 1996; Devlin et al., 1997).

## Indoor exposure to ozone: building and aircraft cabin

Ozone transport from outdoors to indoors via ventilation and infiltration can be emitted by indoor sources such as photocopiers, laser printers, electrostatic precipitators or air filtering devices (Devlin et al., 1997; Weschler, 2000; Poppendieck et al., 2014) such as ozone generators and ionizers. The other important domain of ozone exposure is commercial aircrafts that typically cruise at an altitude of 39,000 ft. In the heights of the upper troposphere or lower stratosphere (Spengler et al., 204), ozone concentrations range from hundreds of ppb to ppm. In addition to

the direct impact of inhalation of ozone, it is also important to consider the effects of ozone derived products on the cabins' occupants. A number of studies have shown that ozone reactions with indoor surfaces and hydrocarbon contaminants (e.g., cleaning/scenting agents) can form formaldehyde, other aldehydes, ketones, and organic acids (National Research Council, 2002). Other than formaldehyde, which is both a carcinogen and a respiratory and ocular irritant, the potential adverse health effects of such compounds include irritations to airway passage, skin and eyes (Clausen et al., 2001; Anderson et al., 2007).

**Breathing zone concentration**

Concentration of ozone in the breathing zone can be significantly lesser than that in the ambient zone of the room due to the chemical reactions between ozone and human skin and clothing surfaces. Contrariwise, an increase in concentration of ozone reaction products associated with human surfaces (ORPHS) in the breathing zone, relative to the concentration in the ambient zone is predicted (Rim et al., 2009). Mass transfer rate of ozone in the human surface boundary layer strongly depends on indoor airflow and surface reactivity (Nazaroff et al., 1993). Such parameters also influence the rate formation of ozone reaction byproducts.

**Ozone mass transfer rate**

In addition to evaluating the breathing zone concentration, the ozone-human reaction can be quantified by another term called mass transfer rate or deposition velocity. A number of studies

pertaining to building as well as aircraft cabin domains have been conducted to record the values of deposition velocity. Such values are recorded in an experimental setup over a range of ventilation rates (Rai et al. (2014), Wisthaler and Weschler (2010), Pandrangi and Morrison (2008), and Tamas et al. (2006)). Rim et al. (2009) and Rai et al. (2012) used computational solvers to find the ozone mass transfer rates in building and aircraft cabin geometries respectively.

The present study uses these measurements to validate the CFD model and conduct a quantitative analysis on the influence of ventilation and surface conditions on ozone uptake to the human surface.

**Objectives**

Based on this background, the objectives of the present study are 1) to investigate ozone reaction with human surfaces depending on indoor ventilation conditions; 2) to examine the breathing zone concentration of ozone considering reactivity of human skin oil and clothing; and 3) to explore the effect of reaction probability on ozone mass transfer rate. Considering the range of indoor environment conditions, the present study examines the effects of indoor airflow and surface reactivity on ozone-surface reaction dynamics.

# Chapter 2

# Methods

Computational fluid dynamics (CFD) simulation is used that is verified and validated by previous ozone model. Grid sensitivity analysis has been performed, using the validated CFD model, deposition velocities and reaction probabilities were calculated for different ventilation conditions and varying degrees of reaction probability. Independent variables included ozone supply concentration and human surface reactivity. The characteristics of ozone reaction with human surface are examined under two representative indoor air flow patterns: momentum-driven flow and buoyancy-driven flow.

## CFD model description

A commercial CFD solver, Star-CCM+ is used to construct the geometry and perform the analysis. The dimensions of the room are 4m x 4m x 3.63m (Figure 2-1). Human geometry of area 1.583 $m^2$ is incorporated into the setup in a seated posture and it represents an ozone sink. This study uses the human geometry modeled by Nilsson et al. (2007).

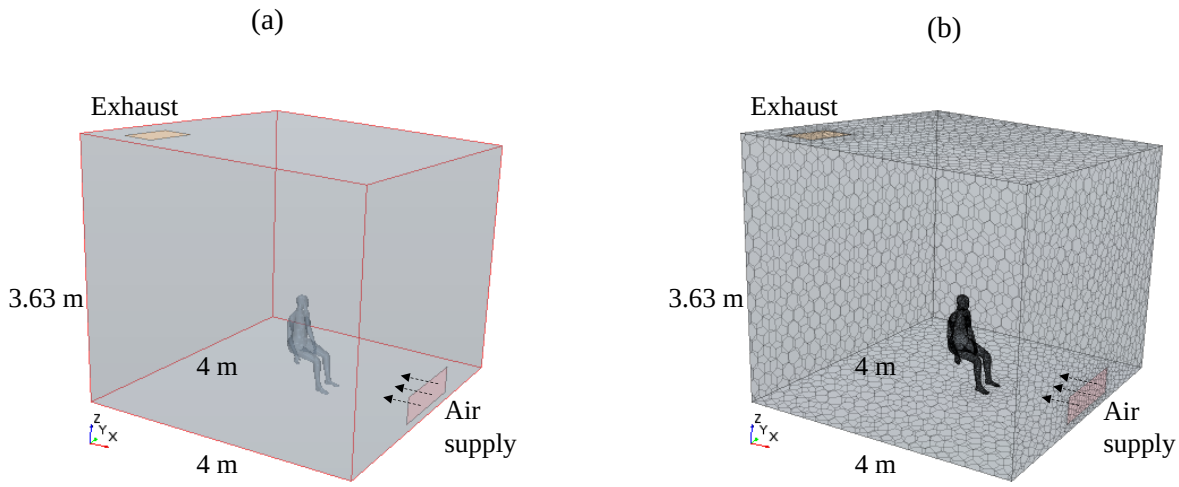


**Figure 2-1:** (a) CFD model of ventilated room (b) mesh

**Grid sensitivity analysis and model validation**

To perform the grid sensitivity analysis, impact of computational grid resolution was studied by comparing four different cell counts cases (50,000, 80,000, 120,000 and 150,000 cells). A polyhedral mesher was used as it can predict local velocity gradient with a reasonable accuracy and handle re-circulating indoor airflow better than tetrahedral mesh. For all the four cases, the human body is of very fine mesh size down to around 10 mm to capture the detailed airflow around the body. The velocities that represent the upward thermal plume are the largest and are measured at eight point probes covering a horizontal circular area of diameter 0.25 m above the head. A surface averaged velocity is also calculated to avoid inaccuracy that occurs due to large velocity gradients within the plume (Rim and Novoselac, 2009). Figure 2-2 shows that grid resolution has a minimal influence on vertical velocity above the head.

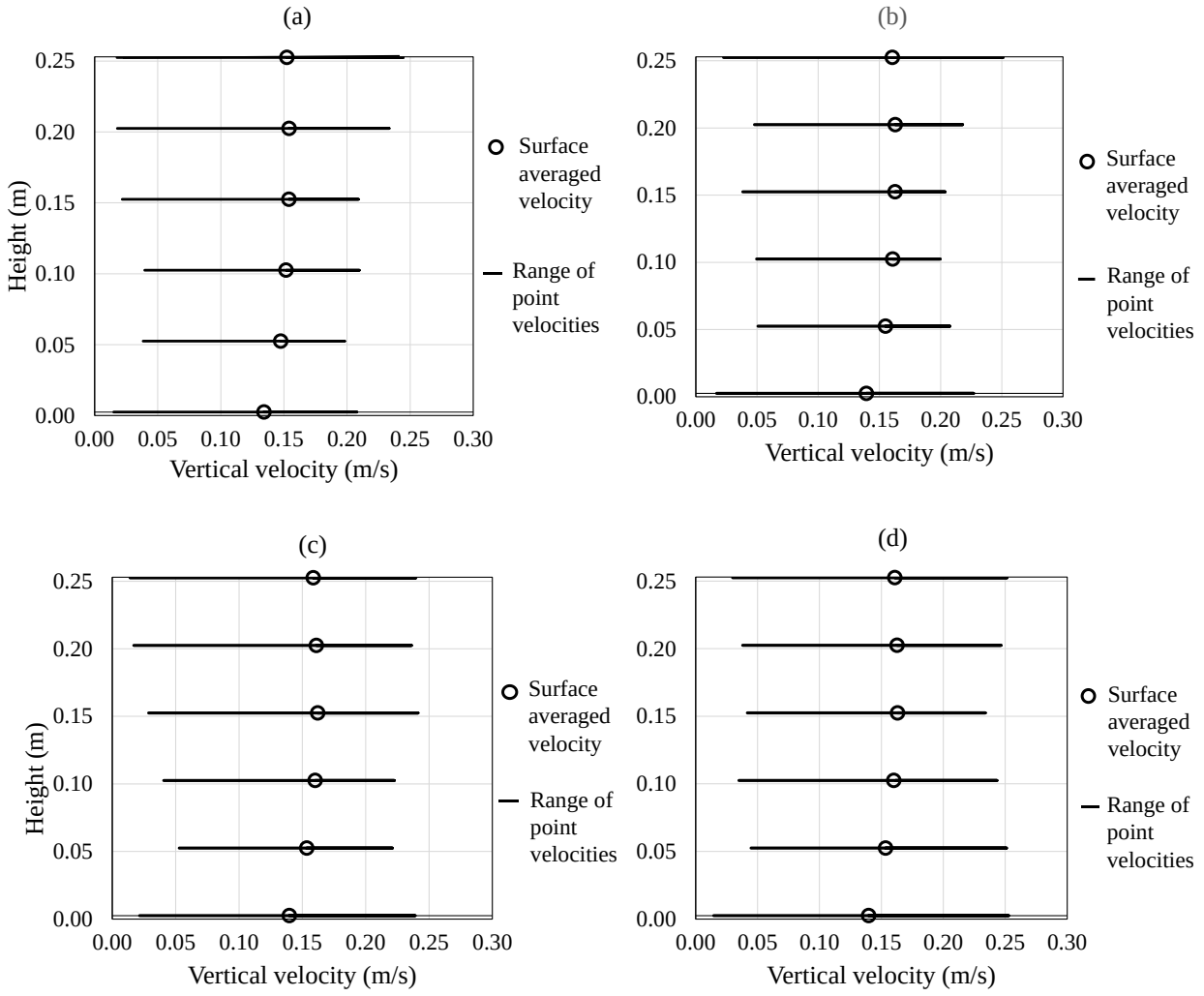
(a)
(b)
(c)
(d)
Height (m)
Vertical velocity (m/s)
0.00
0.05
0.10
0.15
0.20
0.25
0.30
Surface averaged velocity
Range of point velocities

(e)

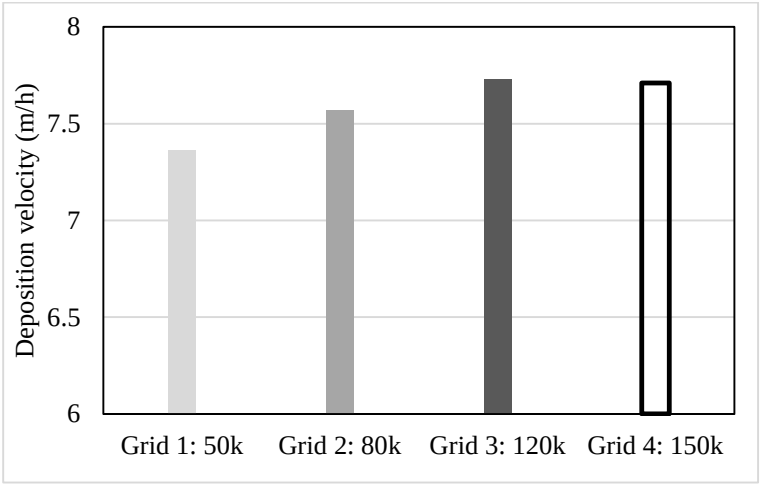


**Figure 2-2:** Simulation with ventilation rate of 1 $h^{-1}$ and perfect sink condition at human surface: vertical (z-axis) velocity profile 25 cm above head for grids of cell sizes (a) 50k (b) 80k (c) 120k (d) 150k; and (e) mass transfer coefficients

With regard to mass transfer coefficient, the ozone deposition velocity is calculated. It is determined from Equation (1).

$$v_d = \frac{(C_s - C_{ex}) \times Q}{C_b \times A_h} \quad (1)$$

In Equation (1), $v_d$ = deposition velocity (m/h), $C_s$ = supply ozone concentration (ppb), $C_{ex}$ = exhaust ozone concentration, $C_b$ = bulk/ambient ozone concentration, $Q$ = volumetric flow rate ($m^3$/h), and $A_h$ = area of human surface ($m^2$). Note that $C_b$ is calculated as the surface averaged ozone concentration over a hollow cuboid in a vertical plane 1 m away from the occupant on all four sides.

It ranged from 7.36 m/h to 7.73 m/h for the four grid sizes, with the gradient decaying beyond 120,000 cell size. The calculated range of values agrees well with other experimental and

computational studies under somewhat similar ventilation and occupancy conditions, in particular, Rai et al. (2014), Rim et al. (2009) and Pandrangi and Morrison (2008) as shown in Table 2-1.

**Table 2-1:** Results from literature

| Author(s) | Method | Study domain | Airflow pattern | Air exchange rates ($h^{-1}$) | No. of people | Surface condition | Ozone deposition velocity (m/h) |
|---|---|---|---|---|---|---|---|
| Rai et al. (2014) | Experiment | Building | Ceiling supply | 0.5 - 2.7 | 1 | Clothing | 5.4 - 10.4 |
| Rai et al. (2012) | CFD | Aircraft cabin | Ceiling supply | 8.8 | 21 | Perfect ozone sink | 11.88 |
| Wisthaler and Weschler (2010) | Experiment | Building | - | 1 | 2 | Skin oil and clothing | 14.4 - 18 |
| Rim et al. (2009) | CFD | Building | Floor supply | 0.8 | 1 | Perfect ozone sink | 6.98 |
| Pandrangi and Morrison (2008) | Experiment | Building | - | 0.3 | 1 | Skin oil and clothing | 6.6 - 30 |
| Tamas et al. (2006) | Experiment | Aircraft cabin | Ceiling supply | 3 - 8.8 | 16 | Skin oil and clothing | Passengers: 7.2 - 8.3; Soiled T-shirts: 6.8 - 9.7 |

Based on the grid sensitivity analysis, the total mesh count of 120,000 with base cell sizes of 0.01 m for human surface and 0.1 m for ambient region was adopted. Using this mesh condition, steady state simulations were performed to capture the effects of buoyancy and thermal stratification. The transport of a mixture of air and ozone was solved based on a balance of heat and mass in each cell. Considering the variation of pressure and flow velocity in the indoor space due to turbulence, the SST k-w turbulence model was used. Gilani et al. (2016) reported that the SST k-w turbulence model produces the appropriate results that match with the experimental data for indoor air ventilation applications. Also, it captures the thermal stratification and reproduces the turbulent thermal plume better than k-ε models.

**Simulation of ozone-surface reaction depending on airflow condition**

The validated CFD model revealed dynamic behavior of ozone in the human surface boundary layer under two representative indoor airflow conditions: floor air supply vs. ceiling air supply. For the floor supply case (Figure 2-3a), conditioned air is supplied at floor level with a low momentum, driven to the upper zone by the occupant thermal plume, and exhausted at ceiling height. The flow is thus buoyancy-driven. This type of ventilation is prevalent in residential buildings. For the ceiling supply case (Figure 2-3b), conditioned air is supplied at the ceiling level with a high momentum to achieve good air mixing in the room. Hence, it is a momentum-driven ventilation strategy. Aircraft cabins and office spaces commonly employ this ventilation type.

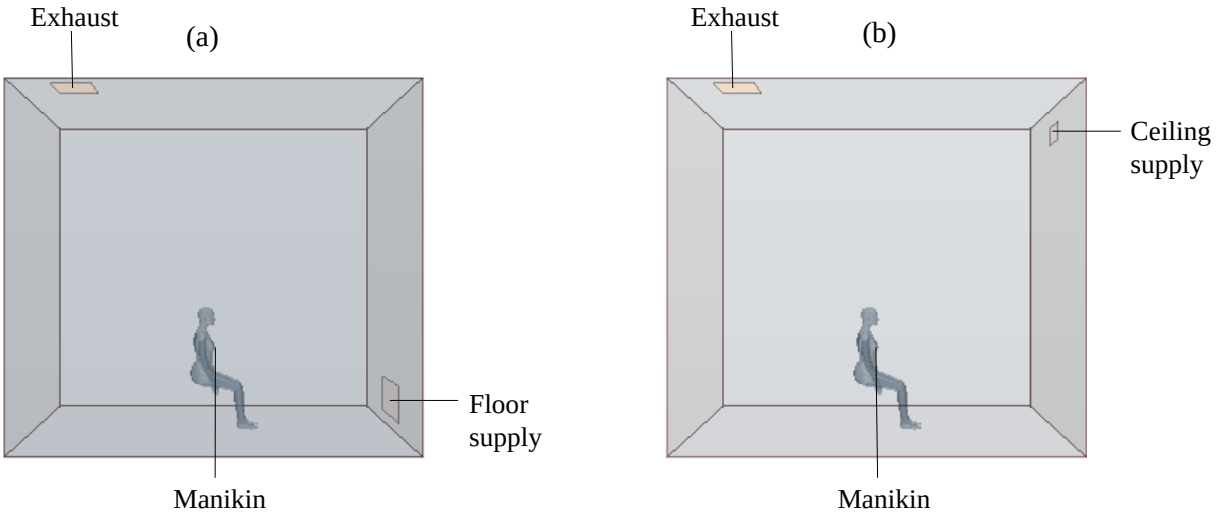


**Figure 2-3:** (a) floor air supply (b) ceiling air supply

The two representative indoor air flow patterns were analyzed with four different air change rates (1, 3, 5 and 10) and three cases of ozone concentrations at the human surface (0 ppb, 20 ppb and

80 ppb), thereby making a total of 24 cases. Air change rate is defined as the rate that room air is replaced with the supply air per hour. The three values of ozone concentrations at the human surface simulate varying degrees of surface reactivity for human and clothing surfaces. For example, the condition of clothes and human skin after an intense workout would correspond to a perfect sink for the ozone to react since the uptake of ozone to skin and clothing coated with skin oils is nearly transport limited (Cano-Ruiz et al., 1993; Pandrangi & Morrison, 2008). The concentration of ozone at those human related surfaces is expected to be very low (0 ppb) as ozone reacts significantly with human skin oils (Pandrangi and Morrison, 2008; Wisthaler and Weschler, 2010). Similarly, an ozone concentration of 80 ppb at the human surface simulates a situation where there is less organic molecules on the body and clothes.

For the total 24 cases, temperature and air flow distribution, age-of-air, breathing zone concentration, and ozone deposition velocity were examined.

**Table 2-2:** Boundary conditions

| | |
|---|---|
| Supply ozone concentration (ppb) | 100 |
| Area of human surface ($m^2$) | 1.583 |
| Room volume ($m^3$) | 58.08 (4x4x3.63) |
| Supply area ($m^2$) | 0.48 (floor supply); 0.12 (ceiling supply) |
| Supply air temperature (°C) | 17 |
| Convective heat transfer from the body (W) | 38 |
| Radiative heat transfer from the body (W) | 30 |
| Ozone concentration at the human surface (ppb) | 0, 20, 80 |

Age of air is one of the parameters used for evaluating ventilation effectiveness and indoor air quality. Age of air is defined as the time it takes for outdoor air to reach a particular location within the indoor environment (Sandberg, 1981). To quantify the age of air, sulfur hexafluoride ($SF_6$) was used in this simulation as the tracer-gas. With a continuous and uniform emission rate of 1.0E-07 kg/m$^3$.s, tracer gas concentration at a given point reveals the freshness of the air. Age of air was calculated based on Equation (2) defined below.

For a room with single pair of supply and exhaust systems with uniform and continuous contaminant generation, Equation (2) gives the calculation for age of air (Kato and Yang, 2008).

$$A_i = \frac{C_i \times 60}{C_{ex} \times ACH} \qquad (2)$$

In Equation (2), $A_i$ = age of air in minutes at location $i$, $C_i$ = mole fraction of $SF_6$ at location $i$, $C_{ex}$ = mole fraction of $SF_6$ at the exhaust, and $ACH$ is the air exchange rate per hour.

The air coming from the inlet would be entirely fresh; therefore age of air at the supply diffuser is zero. However, age of air in any stagnant zone can be higher than ambient zone, representing a polluted zone.

**Surface reaction probability**

The deposition velocity was further parameterized through resistance-uptake theory that models ozone uptake to a surface as the sum of serial resistances describing two governing processes: transport to the surface and surface reaction kinetics, as shown in Equation (3) (Cano-Ruiz et al., 1993).

$$\frac{1}{v_d} = \frac{1}{v_t} + \frac{4}{\gamma\langle v\rangle} \quad (3)$$

In Equation (3), $v_t$ = transport-limited deposition velocity (cm/s), $\gamma$ = reaction probability, and $\langle v\rangle$ is the Boltzmann velocity for ozone ($3.61\times10^4$ cm/s and $3.64\times10^4$ cm/s for 22 °C and 28 °C, respectively).

In this study, the transport-limited deposition velocity ($v_t$) was evaluated by treating the human surface as a perfect ozone sink (zero concentration at the surface). Based on the assumption that ozone uptake to the human surface is limited by external mass-transfer, the deposition velocity of ozone to the perfect ozone sink surface ($v_d$) can be equated to the mass-transport-limited deposition velocity ($v_t$). According to Equation (3), the deposition velocity varies with the surface reaction probability, $\gamma$. This reaction probability is defined as the fractional likelihood of a reaction given a collision between a surface and ozone. In this study, reaction probabilities were calculated for three surface conditions (0, 20, and 80 ppb ozone concentrations at the human surface). Under the same indoor airflow condition, $\gamma$ for 0 ppb at the surface would simulate ozone sink condition thereby yielding the highest reaction probability while $\gamma$ for 80 ppb at the surface will have the lowest reaction probability.

# Chapter 3

# Results and discussion

This section is organized into four subsections. I present 1) the air flow distribution, temperature and age of air in the vicinity of human body at 5 ACH and 2) deposition velocity. The next subsection presents 3) the effects of surface reactivity on deposition velocity followed by 4) breathing zone ozone concentration.

## Air flow distribution, temperature and age of air in the vicinity of human body

Since heat and mass transfer around human body strongly depend on indoor air flow pattern, it is important to compare air velocity distribution (Figures 3-1a and 3-1b). In the case of buoyancy-driven ventilation, the thermal plume is dominant. Based on Figure 3-1a, it is evident that the air velocity is the highest above the head of the simulated occupant, which is up to 0.24-0.28 m/s and higher than incoming supply air velocity (0.17 m/s) or ambient velocity (0.02-0.07 m/s).

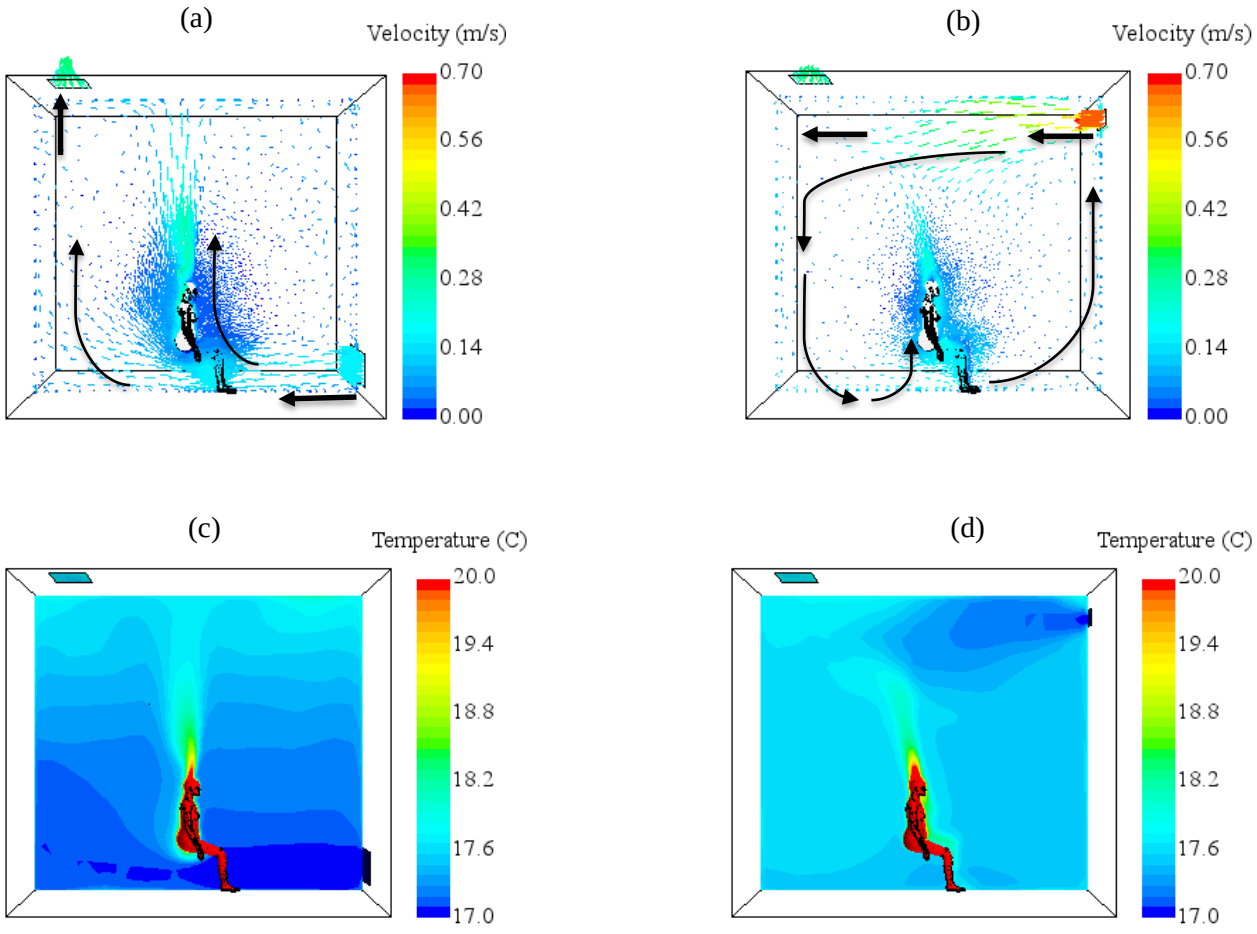


**Figure 3-1:** Velocity distribution (a) buoyancy-driven flow (b) momentum-driven flow; temperature distribution (c) buoyancy-driven flow (d) momentum-driven flow

In the case of momentum-driven flow (Figure 3-1b), the supply air velocity is the highest (0.67 m/s) and it flows along the wall surfaces. This air circulating pattern promotes efficient mixing in the room. The air velocity is almost constant at an average value of 0.10 m/s throughout the occupied zone owing to air mixing caused by the incoming supply jets. These simulated results agree with airflow characteristics observed in several experimental and numerical studies (Cheng et al., 2015; Rim et al., 2009).

The effects of air flow distribution are fittingly observed in the thermal gradient contours (Figures 3-1c and 3-1d). The dominant plume generates stratified thermal layers owing to buoyancy effects (Figure 3-1c). The surface averaged ambient temperature is about 17.2 °C. Figure 3-1d shows that the thermal plume is deflected, although not disrupted entirely. However, because of well-mixing characteristic of momentum-driven ventilation, temperature is uniform around the occupant with a slightly higher average ambient temperature of 17.6 °C.

Figure 3-2 shows distribution of age of air in the two airflow patterns. It reveals that in the breathing zone, air is fresher (9-10 min) in buoyancy driven flow compared to momentum-driven flow (13-14 min) at the same air change rate of 5 $h^{-1}$. This pattern agrees with the finding by Zhang et al. (2005) that air is fresher in the breathing zone with displacement ventilation (buoyancy-driven) than mixing ventilation (momentum-driven). The thermal plume from the human body draws fresh air supplied at the floor level to the breathing zone.

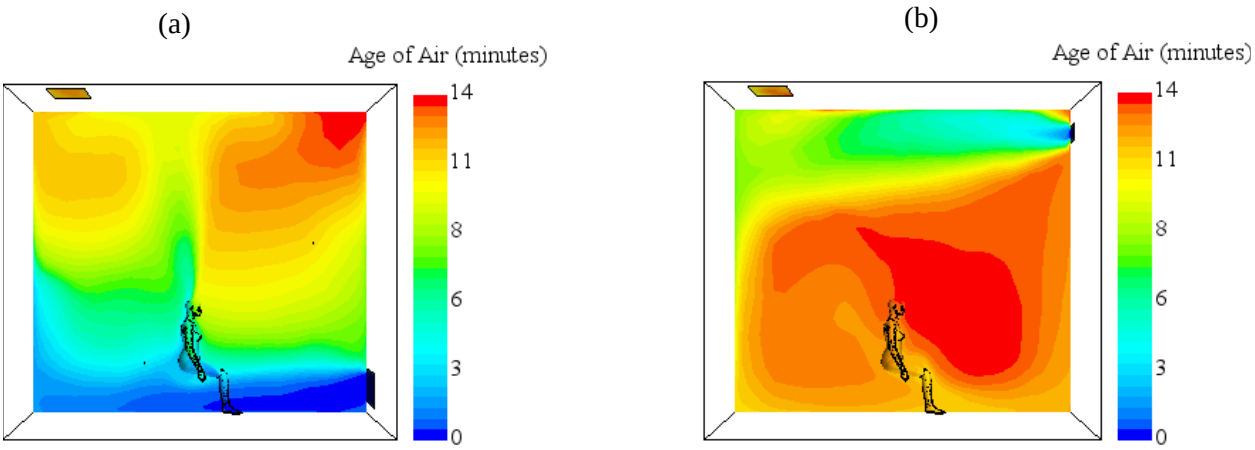


**Figure 3-2**: Age of air (a) buoyancy-driven flow (b) momentum-driven flow

**Deposition velocity**

Figure 3-3 shows ozone deposition velocity for the reactive human surface under two ventilation strategies. Figures 3-3a and 3-3b demonstrate that ozone mass transfer rate (or deposition velocity) varies with ventilation rate and surface reactivity. Ventilation strategy has a marginal influence on the ozone deposition velocity due to reactive human surface. Overall, surface reactivity has a greater effect on the mass transfer compared to ventilation rate. With the perfect ozone sink condition (0 ppb at the occupant surface), ozone deposition velocity ranges between 8 and 10 m/h. This pattern is robust over a wide range of ventilation rates (1-10 $h^{-1}$) under both buoyancy-driven flow and momentum-driven flow. However, ozone deposition velocity is only about 2 m/h with a reduced surface reactivity at the 80 ppb ozone concentration at the human surface. This trend suggests that surface reactivity has significant impact on the rate of ozone mass transfer, accordingly the ozone consumption and formation of reaction products

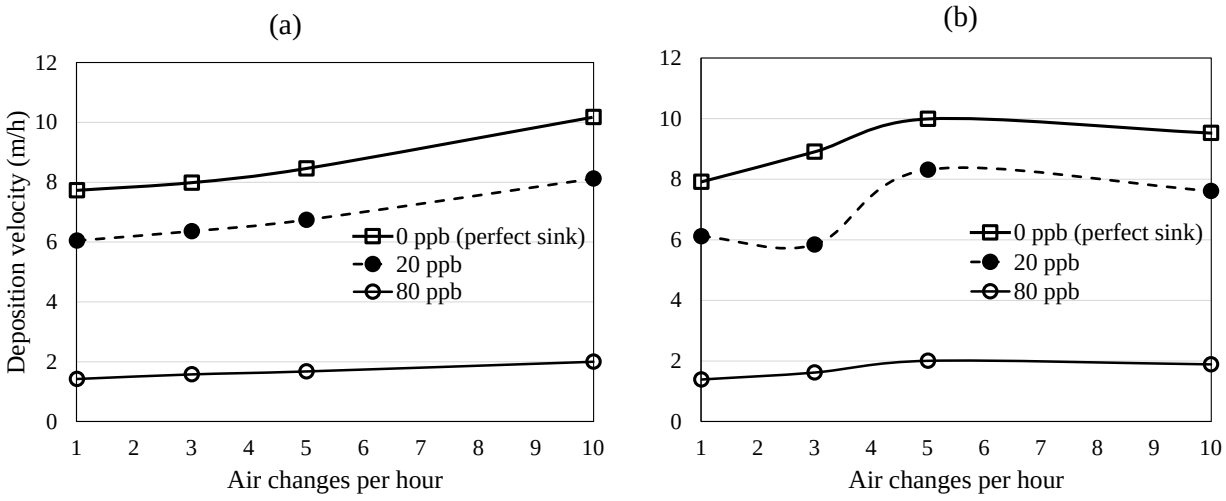


**Figure 3-3:** Deposition velocity as a function of ventilation rate (1-10 $h^{-1}$) and surface reactivity (ozone concentration at the occupant surface from 0 to 80 ppb) under (a) buoyancy-driven flow (b) momentum-driven flow

Also, several previous studies reported ozone deposition velocity comparable to the results produced in this study. Tamás et al. (2006) studied ozone deposition velocity for passengers and for T-shirts soiled with human skin oils (proxy for passengers) in a simulated aircraft cabin. The calculated deposition velocities were in the range of 7.2 – 8.3 m/h for the passengers and 6.8 – 9.7 m/h for the soiled T-shirts. Wisthaler and Weschler (2010) reported deposition velocities between 14.4 – 18 m/h for two occupants in a simulated office environment. According to the study by Rai et al. (2014), deposition velocity for a soiled T-shirt varied from 5.4 – 10.4 m/h in an experimental chamber under typical indoor conditions. An increase in deposition velocity was also found with increasing soiling level and ventilation rate. According to the study by Rim et al. (2009), ozone deposition velocity for a human simulator with surface ozone sink was 6.98 m/h, at an air exchange rate of 0.8 $h^{-1}$. The deposition velocity of ozone for passengers in a section of Boeing-767 cabin, at an outdoor airflow rate of 8.8/h, computed by Rai et al. (2012) was 11.88 m/h. Pandrangi and Morrison (2008) obtained an estimate of the ozone deposition velocity to the human surface for a

range of reaction probabilities expected for skin and soiled clothing. It ranged from 6.6 m/h – 30 m/h.

**Effects of surface reactivity on deposition velocity**

In reality, the ozone deposition velocity varies over the human surface condition depending on the amount of skin oil and availability of reactive sites on a given surface. Figure 3-4 exhibits reaction probability for the occupant surface with respect to the ozone concentration at the surface (0 ppb, 20 ppb, and 80 ppb) at an air exchange rate of 5 $h^{-1}$. Transport-limited deposition velocity ($v_t$) is based on the 0 ppb ozone concentration at the surface. 20 ppb at the surface represents the condition limited by transport through the boundary layer, while 80 ppb at the surface indicates the condition limited by the surface reaction.

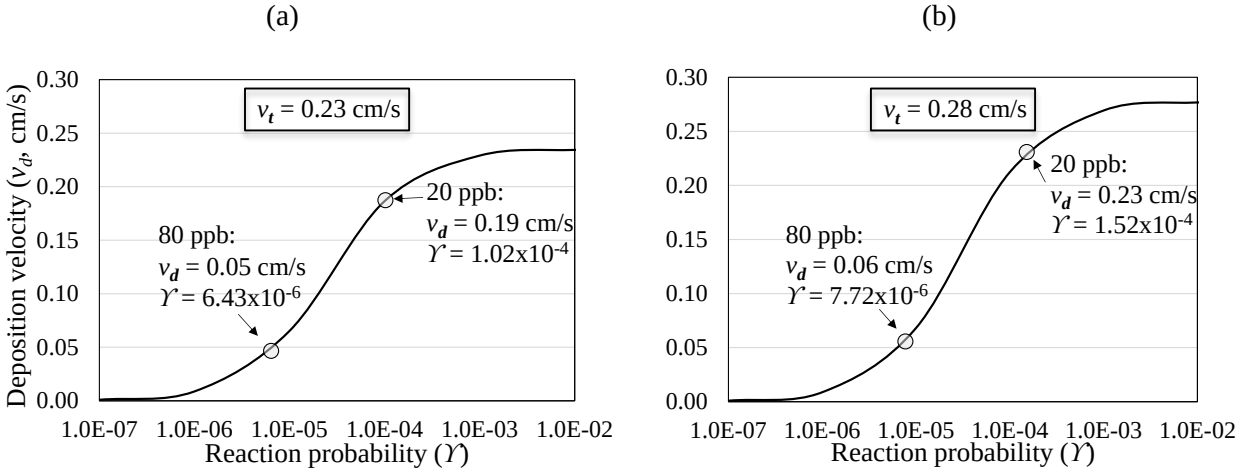


**Figure 3-4:** Effects of surface reactivity on deposition velocity: (a) buoyancy-driven flow (b) momentum-driven flow. Reaction probabilities are calculated based on Equation (3). Note the ventilation rate is 5 $h^{-1}$.

Pandrangi and Morrison (2008) reported that ozone flux to human surface is mainly limited by transport through the boundary layer surrounding the body and reactive sites available on the surface alter the deposition velocity. In their work, the initial and final follicle reaction probability values for hair samples were $(13 \pm 8) \times 10^{-5}$ and $(1.0 \pm 1.3) \times 10^{-5}$. The present study found reaction probabilities of $(8.3 - 15.2) \times 10^{-5}$ for 20 ppb and $(0.52 - 0.76) \times 10^{-5}$ for 80 ppb ozone concentrations at the surface. Coleman et al. (2008) reported a range of $1 \times 10^{-4} – 4 \times 10^{-4}$ for skin, hair and soiled clothing. However, the values calculated for laundered clothing in their study ranged from $1.5 \times 10^{-5} – 8 \times 10^{-5}$.

**Table 3-1:** Summary

| Air supply | Air changes per hour | Deposition velocity (m/h) | Reaction probability | Breathing zone $O_3$ concentration (ppb) | Ambient $O_3$ concentration (ppb) | Exhaust $O_3$ concentration (ppb) |
|---|---|---|---|---|---|---|
| Floor | 1 | 7.73 | 1 | 81.02 | 90.35 | 80.96 |
| | | 6.05 | 8.56E-05 | 84.84 | 92.29 | 84.78 |
| | | 1.42 | 5.37E-06 | 96.21 | 98.07 | 96.20 |
| | 3 | 7.98 | 1 | 94.31 | 98.62 | 92.84 |
| | | 6.36 | 9.63E-05 | 95.44 | 98.90 | 94.28 |
| | | 1.58 | 6.05E-06 | 98.86 | 99.72 | 98.57 |
| | 5 | 8.46 | 1 | 97.73 | 98.98 | 95.44 |
| | | 6.74 | 1.02E-04 | 98.19 | 99.19 | 96.36 |
| | | 1.68 | 6.43E-06 | 99.55 | 99.80 | 99.09 |
| | 10 | 10.18 | 1 | 96.55 | 99.26 | 97.25 |
| | | 8.12 | 1.24E-04 | 97.35 | 99.40 | 97.80 |
| | | 2.00 | 7.65E-06 | 98.84 | 99.85 | 99.46 |
| Ceiling | 1 | 7.92 | 1 | 80.45 | 85.16 | 81.62 |
| | | 6.11 | 8.26E-05 | 84.38 | 88.14 | 85.31 |
| | | 1.39 | 5.18E-06 | 96.09 | 97.04 | 96.33 |
| | 3 | 8.91 | 1 | 88.61 | 94.06 | 92.39 |
| | | 5.84 | 5.22E-05 | 92.32 | 95.49 | 94.93 |
| | | 1.62 | 6.09E-06 | 97.11 | 98.90 | 98.55 |
| | 5 | 9.99 | 1 | 84.85 | 96.01 | 94.77 |
| | | 8.31 | 1.52E-04 | 92.39 | 96.54 | 95.62 |
| | | 2.00 | 7.72E-06 | 97.53 | 99.21 | 98.92 |
| | 10 | 9.52 | 1 | 81.16 | 96.83 | 97.49 |
| | | 7.61 | 1.17E-04 | 90.72 | 97.37 | 97.98 |
| | | 1.89 | 7.24E-06 | 97.48 | 99.33 | 99.49 |

**Breathing zone ozone concentrations**

Figure 3-5 provides detailed breathing zone concentrations under buoyancy-driven and momentum-driven ventilation. The breathing zone concentration is calculated as the volume averaged concentration over a cube of volume 500 $cm^3$ below the manikin's nose tip (Rim et al. 2009).

Figures 3-5a and 3-5b show that that breathing concentration is sensitive to 1) ventilation strategy, 2) ventilation rate, and 3) surface reactivity. Under the buoyancy-driven ventilation (Figure 3-5a), breathing zone concentration increases as ventilation rate goes up to 5 $h^{-1}$ . For the condition < 5 $h^{-1}$ (which is typical of spaces in buildings), thermal plume is dominant for ozone transport around the body and ozone concentration gradient exist near the breathing zone. In this circumstance, surface reactivity has discernable effect on the breathing zone concentration with the biggest impact with the lowest ventilation rate (1 $h^{-1}$). However, as the ventilation rate is > 5 $h^{-1}$ (See below Figure 3-6e), impact of surface reactivity becomes marginal because the air supplied from the floor sweeps to the front body surface. In this case, the concentration boundary layer near the breathing zone becomes extremely thin, making the breathing zone concentration almost same as the supply concentration.

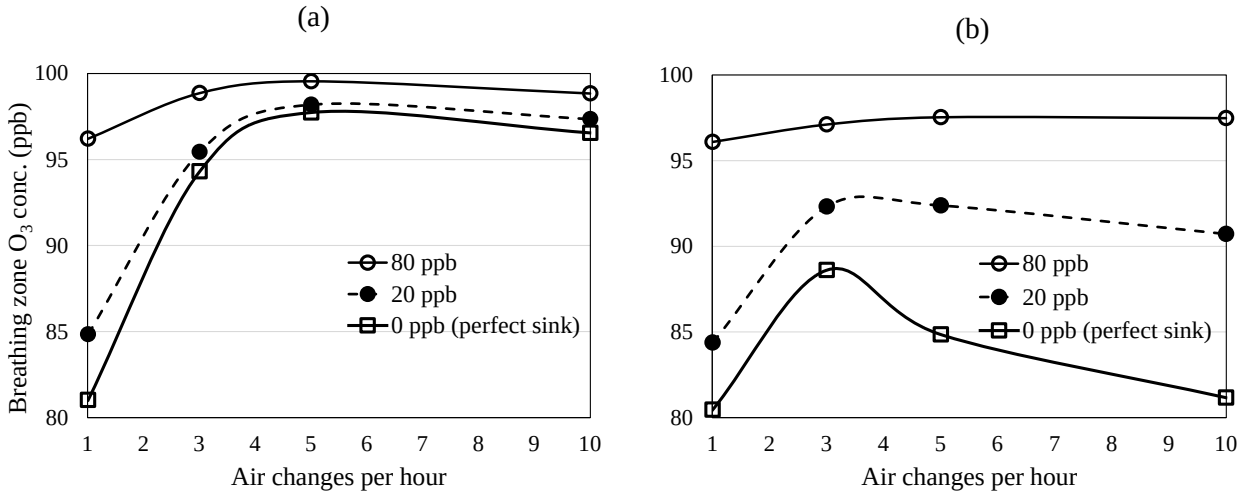


**Figure 3-5:** Breathing zone concentration as a function of ventilation rate (1-10 $h^{-1}$) and surface reactivity (ozone concentration at the occupant surface from 0 to 80 ppb): (a) buoyancy-driven flow (b) momentum-driven flow. Note that the supply ozone concentration is 100 ppb

Under the momentum-driven ventilation (Figures 3-6b, 3-6d and 3-6f), coandă effect occurs and the supply airflow follows the ceiling and wall surfaces. This circulated airflow moves toward the back of the occupant. In this case, the concentration boundary layer near the back of the occupant is very thin; however, near the breathing zone ozone concentration gradient exists. It seems that for the momentum-driven ventilation, surface reactivity plays a significant role on the breathing zone concentration (Figure 3-5b) compared to the buoyancy-driven ventilation. The perfect ozone sink (0 ppb) condition yields notably the lowest breathing zone concentration. This trend suggests that under momentum-driven, circulating airflow, surface reactivity and ventilation rate are equally effective in the breathing zone concentration. Lower breathing zone ozone concentration can occur due to combined effects of surface reactivity and airflow characteristic. This trend agrees well with Rim et al. (2009) where a decrease in breathing zone ozone concentration was reported as

ventilation rate increases higher than 5 $h^{-1}$, although they simulated a different posture of manikin (standing) with a perfect ozone sink condition.

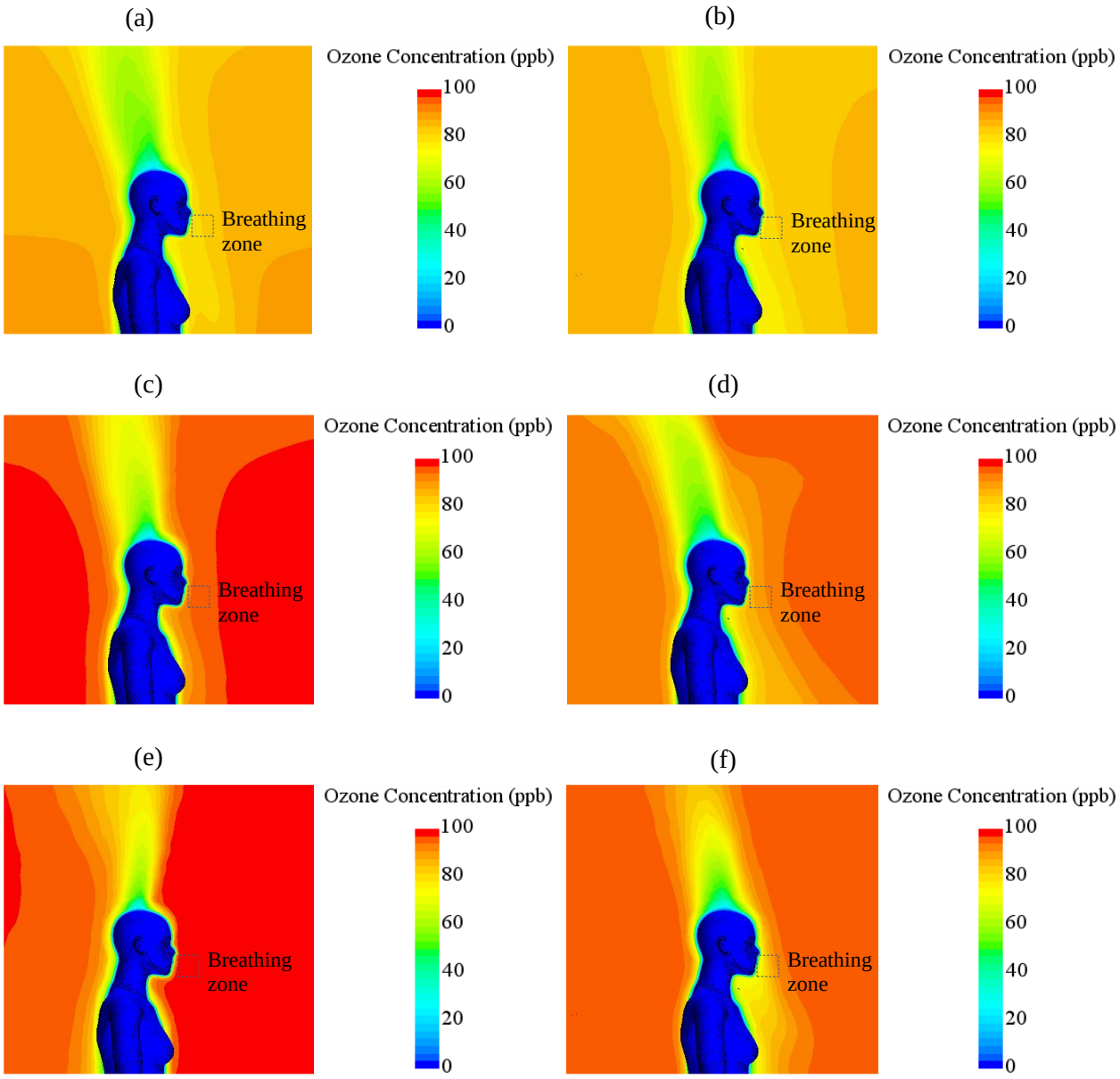


**Figure 3-6:** Ozone concentration near the breathing zone (a) buoyancy-driven flow at 1 $h^{-1}$; (b) momentum-driven flow at 1 $h^{-1}$; (c) buoyancy-driven flow at 3 $h^{-1}$; (d) momentum-driven flow at 3 $h^{-1}$; (e) buoyancy-driven flow at 5 $h^{-1}$; (f) momentum-driven flow at 5 $h^{-1}$. Note that ozone concentration at the human surface is zero representing perfect ozone sink.

# Chapter 4

# Conclusions and future work

This study developed a CFD model to study the influence of indoor air flow conditions and surface reactivity on ozone reaction with human surface thereby acquiring new information with the following conclusions:

- Ozone deposition velocity in an indoor environment (at ventilation rates < 5 $h^{-1}$) is 8-10 m/h with a perfect sink condition
- Surface reactivity of the human body has a larger influence than air change rate and ventilation pattern on ozone mass transfer rate
- Breathing zone concentration increases with ventilation rate in indoor environment (at ventilation rates < 5 $h^{-1}$)
- Breathing zone concentration is in the range of 81-97 ppb under transport-limited condition (human skin oil), while the range is 96-99 ppb with lower surface reaction rate
- Breathing zone concentration is approximately equal to supply ozone concentration beyond five ACH in buoyancy-driven ventilation

While this study provides a detailed parametric analysis on ozone-human reaction under a range of ventilation and surface conditions, the results are greatly affected by the boundary conditions assumed. It is important to remember that heat sources play a significant role in influencing the airflow around the human body and subsequently the concentration of ozone. Hence, any

addition of heat source in the room such as lighting fixture or computer can alter the measurements. Future work can revolve around this study and explore outcomes in an environment that more closely represents an office setup. Also, the position of supply and exhaust diffusers or orientation and posture of the occupant can produce different results. Hence, these factors need to be kept in mind while using this study for validation of any new model.

# References


Anderson, S.E., Wells, J.R., Fedorowicz, A., Butterworth, L.F., Meade, B.J. and Munson, A.E. 2007) Evaluation of the contact and respiratory sensitization potential of volatile organic compounds generated by simulated indoor air chemistry, Toxicol. Sci., 97, 355–363.

Cano-Ruiz, J. A., et al. "Removal of reactive gases at indoor surfaces: Combining mass transport and surface kinetics." *Atmospheric Environment. Part A. General Topics* 27.13 (1993): 2039-2050.

Cheng, Y., and Z. Lin. "Experimental study of airflow characteristics of stratum ventilation in a multi-occupant room with comparison to mixing ventilation and displacement ventilation." *Indoor air* 25.6 (2015): 662-671.

Clausen, P., Wilkins, C.K., Wolkoff, P. and Nielsen, G.D. (2001) Chemical and biological evaluation of a reaction mixture of R-(+)-limonene/ozone - Formation of strong airway irritants, Environ. Int., 26, 511–522.

Coleman, B. K., Destaillats, H., Hodgson, A. T., & Nazaroff, W. W. (2008). Ozone consumption and volatile byproduct formation from surface reactions with aircraft cabin materials and clothing fabrics. *Atmospheric environment*,*42*(4), 642-654.

Comrie, Andrew C. "The climatology of surface ozone in rural areas: a conceptual model." *Progress in Physical Geography* 14.3 (1990): 295-316.

Devlin, Robert B., James A. Raub, and Lawrence J. Folinsbee. "Health effects of ozone." *Science and Medicine* 4 (1997): 8-17.

Gilani, Sara, Hamid Montazeri, and Bert Blocken. "CFD simulation of stratified indoor environment in displacement ventilation: Validation and sensitivity analysis." *Building and Environment* 95 (2016): 299-313.

Kato, Shinsuke, and Jeong-Hoon Yang. "Study on inhaled air quality in a personal air-conditioning environment using new scales of ventilation efficiency." *Building and Environment* 43.4 (2008): 494-507.

Lippmann, Morton. "Health effects of ozone a critical review." *Japca* 39.5 (1989): 672-695.

Lin, Zhang, et al. "Comparison of performances of displacement and mixing ventilations. Part II: indoor air quality." *International Journal of Refrigeration*28.2 (2005): 288-305.

Nazaroff, William W., Ashok J. Gadgil, and Charles J. Weschler. "Critique of the use of deposition velocity in modeling indoor air quality." *Modeling of indoor air quality and exposure*. ASTM International, 1993.

Nilsson, H., H. Brohus, and P. V. Nielsen. "Benchmark test for a computer simulated person–Manikin heat loss for thermal comfort evaluation." *Aalborg University Denmark & Gavle University Sweden* (2007).

NRC (National Research Council), Committee on Air Quality in Passenger Cabins of Commercial Aircraft. (2002) "The Airliner Cabin Environment and the Health of Passengers and Crew", Washington DC: National Academy Press.

Pandrangi, Lakshmi S., and Glenn C. Morrison. "Ozone interactions with human hair: Ozone uptake rates and product formation." *Atmospheric Environment* 42.20 (2008): 5079-5089.

Poppendieck, Dustin G., Donghyun Rim, and Andrew K. Persily. "Ultrafine particle removal and ozone generation by In-duct electrostatic precipitators."*Environmental science & technology* 48.3 (2014): 2067-2074.

Rai, A. C., Guo, B., Lin, C. H., Zhang, J., Pei, J., & Chen, Q. (2014). Ozone reaction with clothing and its initiated VOC emissions in an environmental chamber. *Indoor air*, *24*(1), 49-58.

Rai, Aakash C., and Qingyan Chen. "Simulations of ozone distributions in an aircraft cabin using computational fluid dynamics." *Atmospheric Environment*54 (2012): 348-357.

Rim, D., & Novoselac, A. (2009). Transport of particulate and gaseous pollutants in the vicinity of a human body. *Building and Environment*, *44*(9), 1840-1849.

Rim, D., Novoselec, A., Morrison, G., 2009. The influence of chemical interactions at the human surface on breathing zone levels of reactants and products. Indoor Air 19, 324-334.

Sandberg, M. (1981). What is ventilation efficiency?. *Building and environment*, *16*(2), 123-135.

Spengler, J. D., S. Ludwig, and R. A. Weker. "Ozone exposures during trans-continental and trans-pacific flights." *Indoor Air* 14.s7 (2004): 67-73.

Tamas, G., Weschler, C. J., Bako-Biro, Z., Wyon, D. P., & Strøm-Tejsen, P. (2006). Factors affecting ozone removal rates in a simulated aircraft cabin environment. *Atmospheric Environment*, *40*(32), 6122-6133.

U.S. EPA. 1996. Air Quality Criteria for Ozone and Related Photochemical Oxidants. EPA/600/P-93/004a-cF. Washington, DC:U.S. Environmental Protection Agency

Weschler, C.J. 2000. Ozone in indoor environments: concentration and chemistry. *Indoor Air* 10, 269-288.

Wisthaler, Armin, and Charles J. Weschler. "Reactions of ozone with human skin lipids: sources of carbonyls, dicarbonyls, and hydroxycarbonyls in indoor air." *Proceedings of the National Academy of Sciences* 107.15 (2010): 6568-6575.

# Appendix A

## Mesh for different grid sizes

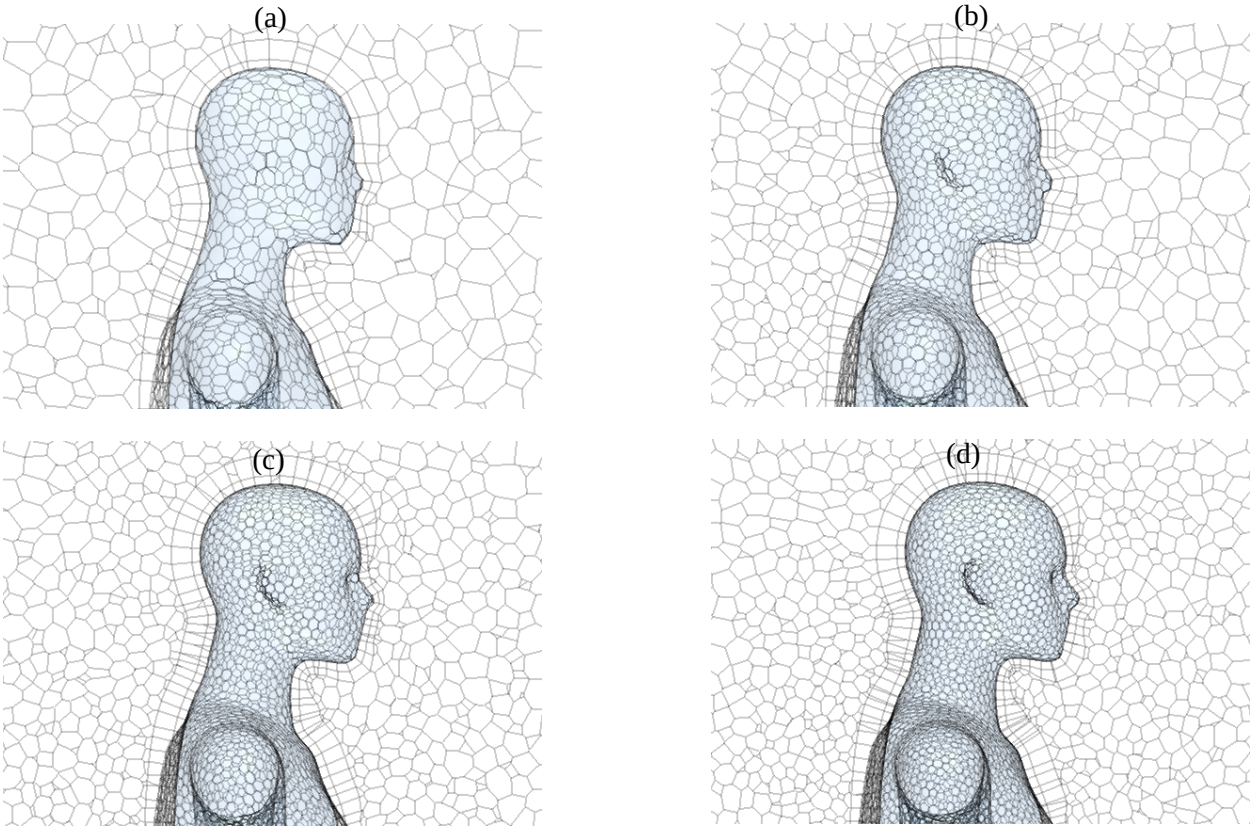


**Figure A-1:** Mesh contours around the human body for grid sizes: (a) 50k (b) 80k (c) 120k and (d) 150k cells

# Appendix B

## Transient ozone concentration

A time-varying simulation is run to compare its results with steady-state simulation. Figure B-1 shows good agreement between the values for bulk ozone concentration observed in the transient case and in Table 3-1.

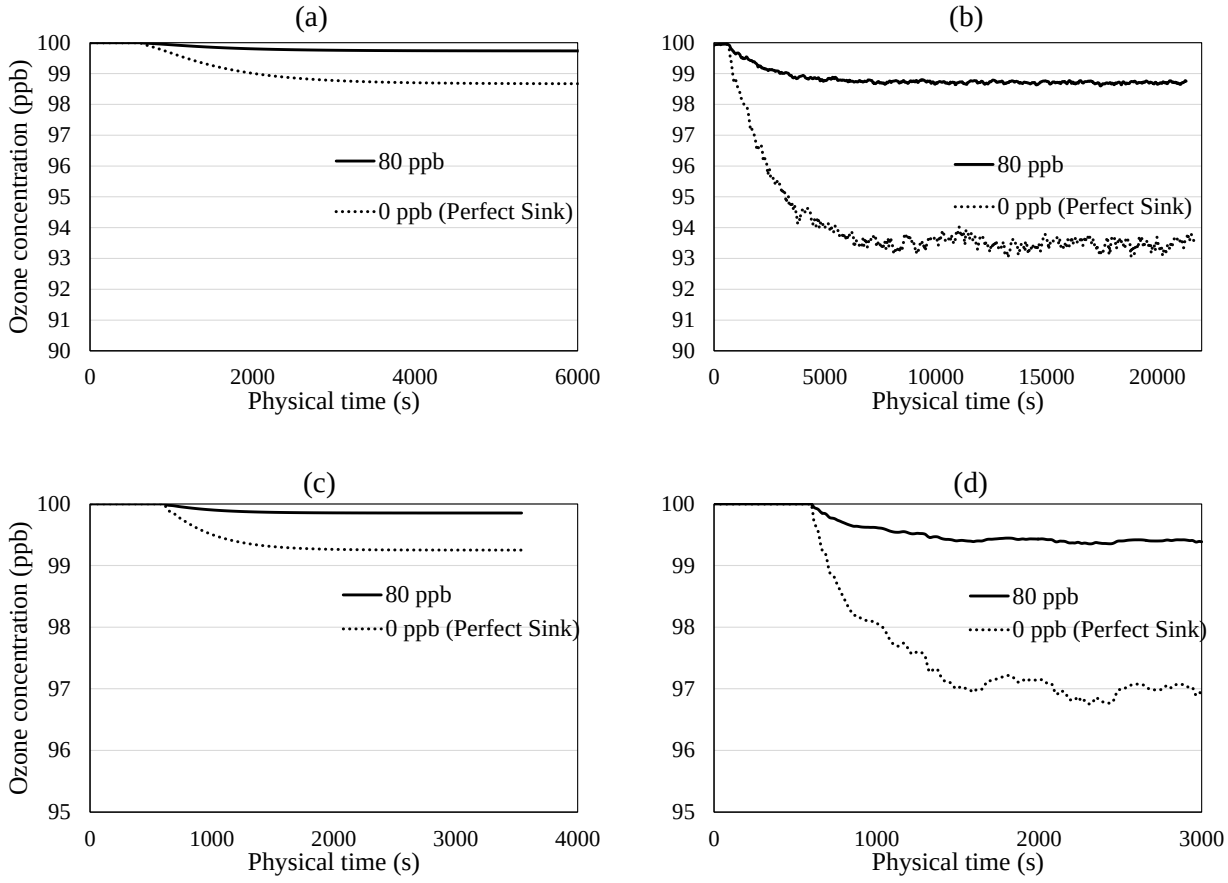


**Figure B-1:** Ambient ozone concentration vs physical time at two surface conditions: (a) buoyancy-driven flow at 3 ACH (b) momentum-driven flow at 3 ACH (c) buoyancy-driven flow at 10 ACH (d) momentum-driven flow at 10 ACH